Acta Biomaterialia 34 (2016) 93–103

Contents lists available at ScienceDirect

Acta Biomaterialia

journal homepage: www.elsevier.com/locate/actabiomat

Full length article

Hydrogel arrays formed via differential wettability patterning enable combinatorial screening of stem cell behavior ☆

Ngoc Nhi T. Le [a], Stefan Zorn [b], Samantha K. Schmitt [a], Padma Gopalan [a,c,d], William L. Murphy [a,b,c,e,*]

[a] Materials Science Program, University of Wisconsin-Madison, Madison, WI, USA
[b] Department of Biomedical Engineering, University of Wisconsin-Madison, Madison, WI, USA
[c] Department of Material Science and Engineering, University of Wisconsin-Madison, Madison, WI, USA
[d] Department of Chemistry, University of Wisconsin-Madison, Madison, WI, USA
[e] Department of Orthopedics and Rehabilitation, University of Wisconsin-Madison, Madison, WI, USA

ARTICLE INFO

Article history:
Received 1 June 2015
Received in revised form 3 September 2015
Accepted 15 September 2015
Available online 16 September 2015

Keywords:
Human mesenchymal stem cell
Cell adhesion
Mechanosensing
RGD peptide
Thiol-ene
Poly(ethylene glycol)

ABSTRACT

Here, we have developed a novel method for forming hydrogel arrays using surfaces patterned with differential wettability. Our method for benchtop array formation is suitable for enhanced-throughput, combinatorial screening of biochemical and biophysical cues from chemically defined cell culture substrates. We demonstrated the ability to generate these arrays without the need for liquid handling systems and screened the combinatorial effects of substrate stiffness and immobilized cell adhesion peptide concentration on human mesenchymal stem cell (hMSC) behavior during short-term 2-dimensional cell culture. Regardless of substrate stiffness, hMSC initial cell attachment, spreading, and proliferation were linearly correlated with immobilized CRGDS peptide concentration. Increasing substrate stiffness also resulted in increased hMSC initial cell attachment, spreading, and proliferation; however, examination of the combinatorial effects of CRGDS peptide concentration and substrate stiffness revealed potential interplay between these distinct substrate signals. Maximal hMSC proliferation seen on substrates with either high stiffness or high CRGDS peptide concentration suggests that some baseline level of cytoskeletal tension was required for hMSC proliferation on hydrogel substrates and that multiple substrate signals could be engineered to work in synergy to promote mechanosensing and regulate cell behavior.

Statement of significance

Our novel array formation method using surfaces patterned with differential wettability offers the advantages of benchtop array formation for 2-dimensional cell cultures and enhanced-throughput screening without the need for liquid handling systems. Hydrogel arrays formed via our method are suitable for screening the influence of chemical (e.g. cell adhesive ligands) and physical (stiffness, size, shape, and thickness) substrate properties on stem cell behavior. The arrays are also fully compatible with commercially available micro-array add-on systems, which allows for simultaneous control of the insoluble and soluble cell culture environment. This study used hydrogel arrays to demonstrate that synergy between cell adhesion and mechanosensing can be used to regulate hMSC behavior.

1. Introduction

It is widely accepted that soluble signals (such as growth factors and cytokines) are major regulatory players in both the *in vivo* and *in vitro* stem cell microenvironments; however, stem cell behavior can also be influenced by a variety of insoluble signals, including biomolecules immobilized in the extracellular matrix as well as biophysical properties of microenvironment [1–3]. Recent studies indicate that regulation of stem cell behavior involves complex relationships between soluble factors, immobilized cell adhesive signals, and mechanical signals contained in, and dynamically regulated by, the stem cell microenvironment. Chemically well-defined cell culture substrates can allow researchers to parse out the effects of specific signals on stem cell behavior [4]. However, attempts to investigate synergistic or antagonistic effects of combinations of signals produce thousands of potential signal

☆ Part of the High Throughput Approaches to Screening Biomaterials Special Issue, edited by Kristopher Kilian and Prabhas Moghe.

* Corresponding author at: Wisconsin Institute for Medical Research II, 1111 Highland Avenue Room 5405, Madison, WI 53705, USA.
E-mail address: wlmurphy@wisc.edu (W.L. Murphy).

http://dx.doi.org/10.1016/j.actbio.2015.09.019
1742-7061/

combinations, leading to difficult and costly experiments [2,5]. Here, we designed hydrogel arrays for enhanced-throughput, combinatorial screening of biochemical and biophysical cues from chemically defined cell culture substrates. Current hydrogel platforms for screening the influence of stiffness on cell behavior rely on low-throughput techniques using bulk hydrogels, plated hydrogel arrays in cell culture dishes or wells, or arrays formed using expensive liquid handling systems. These methods have limitations, including high materials and equipment cost and the potential for deformation via "buckling" when hydrogels swell against the constrained dimensions of the well [2,6–9]. Here, we demonstrated the ability to generate arrays for enhanced-throughput screening without the need for liquid handling systems and our arrays comprise free-standing hydrogel spots, which reduces the likelihood of hydrogel deformation via buckling. Using these arrays, we screened the combinatorial effects of substrate stiffness and immobilized cell adhesion peptide concentration on human mesenchymal stem cell (hMSC) behavior during short-term cell culture. hMSC adhesion was chosen as a model biological outcome to demonstrate the utility of hydrogel arrays, as recent studies have extensively detailed the influence of substrate properties on hMSC behavior [5,10–17].

Over the past two decades, many researchers have demonstrated a positive correlation between the substrate stiffness and the intracellular cytoskeletal tension, indicating that cells sense and respond to changes in matrix stiffness by modulating cytoskeletal assembly and contractility (a concept referred to as "mechanosensing") [11,12]. We and others have also demonstrated control of hMSC behavior by regulating mechanosensing: hMSCs cultured on surfaces that promoted high cytoskeletal tension (via high substrate stiffness, cell adhesion molecule affinity, or cell adhesion molecule density) resulted in well-spread cells that possessed highly-organized F-actin stress fibers and large and well-defined focal adhesions, while substrates that promoted low cytoskeletal tension resulted in rounded cells with diffused actin and small, unstable focal adhesions [5,11,13,18].

2. Materials and methods

2.1. Differential wettability pattering and glass silanization

Gold-coated glass slides (TA134, EMF Corporation) were cleaned via sonication in ethanol for 1 min and dried with air. Hydrophobic SAM formation on gold-coated glass slides were prepared by immersion in a 1 mM solutions of HS–$(CH_2)_{11}$–O–$(CH_2)_2$–$(CF_2)_5$–CF_3 (fluorinated alkanethiols, ProChimia Surfaces) in ethanol for $\geqslant$2 h. Polydimethylsiloxane (PDMS) elastomeric stencils for determining the pattern for selective etching of hydrophilic SAM regions were fabricated using soft lithography as previously described [18] using a 1:10 ratio of curing agent to base. Gold-coated glass slides with the hydrophobic SAM were cleaned with ethanol, dried with air, and covered with the PDMS elastomeric stencil. Exposed regions of the hydrophobic SAM (regions not covered by the PDMS elastomeric stencil) were etched by oxygen plasma treatment at 40 sccm and 50 W for 1 min. The PDMS elastomeric stencil was removed and the selectively etched gold-coated slides were cleaned with ethanol and immersed in a 0.1 mM solution of HS–C_{11}–$(O–CH_2–CH_2)_3$–OH (PEG-terminated alkanethiols, ProChimia Surfaces) in ethanol solution for $\geqslant$2 h so that hydrophilic alkanethiol SAM layer could form in the etched regions. Hydrophobic and hydrophilic SAM formation on the gold-coated slides were confirmed by static contact angles measurements at room temperature using a contact angle goniometer (DataPhysics Contact Angle System, OCA). A drop of distilled water (3 μL) was placed on the surface and the static contact angle was measured for 3 different samples at 5 different places on each sample and the contact angles were averaged.

Silanized glass coverslips were prepared via liquid-phase silanization. Silanization was performed with slight modifications from procedures previously described [19,20]. Glass coverslips were cleaned via sonication in acetone for 30 min, rinse with ethanol, and dried with air. Clean glass coverslips were activated by oxygen plasma treatment at 40 sccm and 50 W for 5 min to increase the number of activated hydroxyl groups on the surface. Immediately after activation, glass coverslips were immersed in a solution of 2.5 v./v.% 3-mercaptopropyl trimethoxysilane (3-MPTS, Sigma Aldrich) in toluene for 2 h, thoroughly rinsed with ethanol, dried with air, cured under nitrogen atmosphere at 100 °C for 1 h, and treated with 10 mM DTT in PBS for 30 min at 37 °C to increase free thiols available for thiolene reaction with PEG-NB.

2.2. Hydrogel array formation

Norbornene-functionalized PEG (PEG-NB, 20 kDa molecular weight, 8-arm with tripentaerythritol core, JenKem Technology) was synthesized and characterized as previously described [21–23]. Dimethylaminopyridine (DMAP), pyridine, dichloromethane (DCM), 5-norbornene-2-carboxylic acid, N,N′-dicyclohexylcarbodiimide (DCC), diethyl ether, hexane, SNAKESKIN dialysis tubing (MWCO 3.5 K), deuterated chloroform ($CDCl_3$), and tetramethylsilane (TMS) were purchased from Sigma Aldrich.

Briefly, eight-arm PEG-OH, DMAP and pyridine (Sigma Aldrich) were dissolved in anhydrous DCM in one reaction vessel and DCC and 5-norbornene-2-carboxylic acid were dissolved in another. The PEG and norbornene solutions were combined and stirred overnight to covalently couple the 5-norbornene-2-carboxylic acid to the PEG-OH. The PEG-NB product was filtered through a medium fritted Buchner funnel to remove urea salts formed during the reaction. The filtrate was then precipitated in 900 mL cold diethyl ether and 100 mL hexane. The solids were collected on qualitative grade filter paper and air dried overnight. The PEG-NB product was purified by dialysis against 4 L of dH2O at 4 °C for 72 h (with water change every 8 h) to remove residual norbornene acid, filtered through a 0.45 μm nylon filter to remove particulates and impurities, and subsequently freeze dried.

Norbornene functionalization of >90% was confirmed with 1H nuclear magnetic resonance spectroscopy. Samples were prepared at 6 mg/mL in $CDCl_3$ with TMS internal standard. Free induction decay (FID) spectra were obtained using spectroscopy services provided by the National Magnetic Resonance Facility at Madison on a Bruker Instruments Avance III 500i spectrometer at 400 MHz and 27 °C.

Linear CRGDS, linear CRDGS, cyclic (RGDfC), and matrix metalloproteinase (MMP)-degradable peptide crosslinker KCGGPQGIW GQGCK were purchased from GenScript USA. Linear PEG-dithiol (PEG-DT, 3.4 kDa) was purchased from Laysan Bio. Note that the "f" notation denotes a D-amino acid.

Hydrogel precursor solutions were prepared by combining PEG-NB (4–8 wt/wt%), PEG-DT (0.5–1 mol ratio of thiol-to-norbornene), peptides (1–4 mM), and 0.5 wt/wt% Irgacure 2959 photoinitiator (CIBA/BASF) and diluted to desired concentrations with phosphate buffered saline (PBS, pH 7.4) immediately prior to hydrogel array formation. For cell encapsulation studies, cells were suspended at the desired concentration in growth medium and added to the remaining hydrogel precursor solution components in place of the PBS that was used for dilution. All encapsulation studies utilized the MMP-degradable crosslinker in place of the non-degradable PEG-DT crosslinker. Hydrogel precursor solutions were spotted onto the hydrophilic regions of the patterned gold-coated slides using a micropipette, the DTT-treated silanized glass

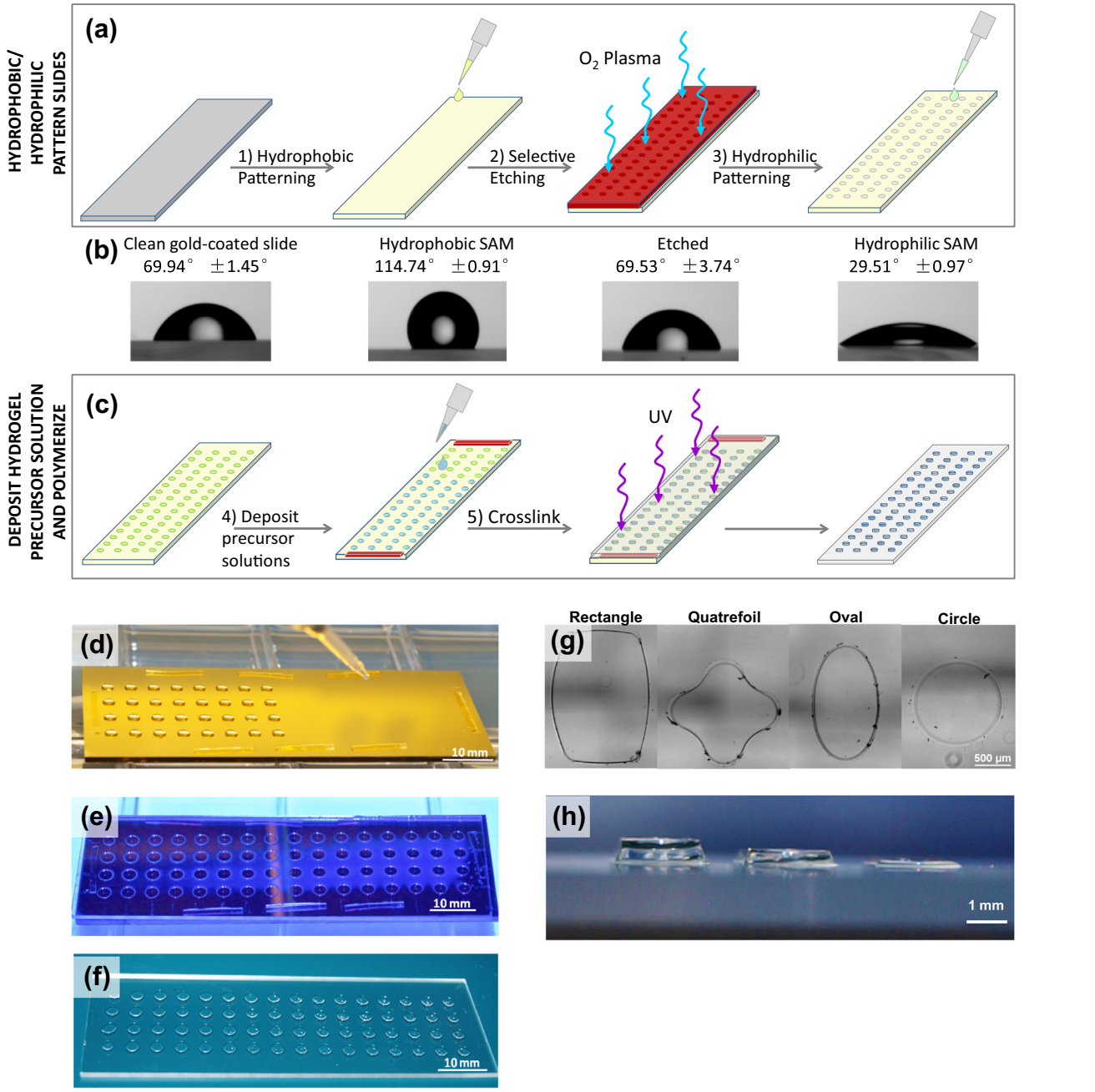

Fig. 1. Hydrogel array formation procedure and outputs. (a and b) Hydrogels arrays were formed on gold-coated glass slides patterned with SAMs with differential wettability. (c–e) Hydrogel precursor solutions deposited onto the hydrophilic SAM regions of the patterned slide were crosslinked via UV-initiated photopolymerization to form hydrogel spots. (f) The resulting array is composed of hydrogel spots immobilized on a glass slide. (g and h) The array formation procedure allows for the formation of hydrogel spots of various size, shape, and height.

coverslip was used to sandwich the hydrogel precursor solutions between the coverslip and the patterned gold-coated slide. Hydrogel precursor solutions were crosslinked by UV-initiated photopolymerization with 365 nm wavelength light for 2 s at 90 mW/cm^2, with the light penetrating through the glass coverslip. The gold-coated slide was separated from the coverslip, which enabled the glass-immobilized hydrogel spots to cleanly detach from the gold-coated slide. The resulting glass-immobilized hydrogel spots, collectively referred to as the "hydrogel array", were allowed to swell to equilibrium overnight at room temperature in PBS, sterilized by immersion in 70% ethanol for $\geqslant$1 h, thoroughly washed with PBS to remove any remaining unreacted components, and immersed in cell growth medium at 37 °C until use.

2.3. Hydrogel array characterization

Hydrogel mass equilibrium swelling ratios [21,23], shear storage moduli [21], and mesh size calculations (calculated using empirical equilibrium swelling data and Flory–Rehner theory) were determined as previously reported [21,24–26]. To characterize surface roughness, hydrogels were allowed to swell to equilibrium in PBS overnight at room temperature then imaged on a BioScope Catalyst BioAFM (Bruker) with a Zeiss optical microscope. Tapping atomic force microscopy (AFM) was performed in ScanAsyst mode in water using ScanAsyst Fluid+ tips (Bruker). At least 3 images of 2.5 µm by 2.5 µm or larger in area were scanned at different locations on the hydrogels and these images were used to calculate height data. The root mean square (RMS) roughness

was calculated using Nanoscope Analysis software (Bruker) for 3 images per sample and averaged.

To demonstrate controllable microsphere encapsulation and peptide immobilization, we formed hydrogel arrays with varying concentrations of 2 μm fluorescent red carboxylate-modified polystyrene latex beads (Sigma Aldrich) and CRGDS peptides in the hydrogel precursor solution. Immediately following hydrogel array formation, the N-terminal amine on CRGDS peptides were labeled using Alexa-Fluor 488 5-sulfodichlorophenol (SDP) ester (Invitrogen) as previously described [21]. Briefly, hydrogel arrays were immersed overnight in a solution of SDP ester in PBS (pH 7.4) with at 2-fold molar excess of SDP ester to CRGDS, rinsed with PBS, soaked in PBS for 6 h with PBS change every 2 h to remove unreacted SDP ester. Fluorescently-labeled arrays were imaged using a Nikon Eclipse Ti microscope (Nikon) and relative fluorescence intensities of each hydrogel spot in the array were obtained using the threshold feature in NIS Elements software (Nikon).

2.4. Cell culture

Bone marrow-derived hMSCs (Lonza) were expanded in 10% fetal bovine serum (FBS, Invitrogen) in minimum essential medium, alpha (αMEM, MediaTech) supplemented with 1% penicillin/streptomycin (Invitrogen) on tissue culture polystyrene plates at 37 °C in a 5% CO_2 atmosphere until 70% confluence. Passage 7 hMSC were harvested using trypsin (Invitrogen), resuspended in 10% FBS in αMEM, and seeded at 2000 cells/cm^2 on sterilized hydrogel arrays. After 24 h, unattached cells were removed by gently replacing the culture media. Cells on hydrogel arrays were maintained at 37 °C in a 5% CO_2 atmosphere and culture media was replaced every 3 days.

2.5. Data acquisition and analysis

Samples were placed in a heated environmental chamber and imaged on the Nikon Eclipse Ti microscope (Nikon) at the desired times. Immunofluorescence staining for vinculin and F-actin were conducted using the FAK100 focal adhesion staining kit (Millipore) per the manufacturer's instructions with 1:200 dilutions of both the TRITC-conjugated phalloidin and primary mouse anti-vinculin monoclonal antibody components included in the kit. Alexa-Fluor 488 goat anti-mouse IgG secondary antibody (Invitrogen) was used at 1:200 dilution. Live/dead stain (Invitrogen) was performed per the manufacturer's instructions. Nuclear counterstain was performed using 1:5000 dilution of diamidino-2-phenylindole (DAPI, Life Technologies).

Cell number was manually determined using NIS Elements software (Nikon), cell area of single cells were determined using NIS Elements's threshold and automated measurement features, and cell proliferation was quantified as previously reported by normalizing cell number at day 4 (C_4) to cell number at day 1 (C_1), where normalized cell number greater than 1 was used to indicate proliferation [18]. Focal adhesion length was determined using NIS Element's threshold and automated measurement features to define regions on the periphery of single cells stained with mouse anti-vinculin monoclonal antibody. Focal adhesion density was determined by normalizing the number features stained with mouse anti-vinculin monoclonal antibody to the cell area. Encapsulated cell concentration was determined by counting cells at 3 focal planes 50 μm apart in distance. Cell viability was determined by comparing the total number of calcein positive to total DAPI positive cells. Statistical analysis was performed using Student's *t*-test (2-tailed, $\alpha = 0.05$) or ANOVA with post hoc Tukey (HSD or Kramer depending on sample size variability) tests as indicated. All error bars denote standard deviation. All Pearson's product-moment correlation coefficients (R^2) were calculated using Excel's Analysis ToolPak.

3. Results and discussion

3.1. Differential wettability patterning and hydrogel array formation

Since cell structural measures (e.g. cell area and morphology) and perturbations (e.g. proliferation and cytoskeletal organization) have been demonstrated to be accurate qualitative measures of hMSC mechanosensing in response to substrate stiffness and ligand density, we examined these properties here using automated data collection techniques that augmented the enhanced-throughput capability of our array-based screening system [11,12,15,24]. Hydrogel arrays were formed using gold-coated glass slides patterned with alkanethiolate self-assembled monolayers (SAMs), and differential wettability was used to define the geometry and confine the contents of each spot in the array (Fig. 1). Gold-coated glass slides with a fully formed hydrophobic SAM composed of fluorinated alkanethiolates were covered with elastomeric stencils and etched using oxygen plasma to selectively destroy exposed regions of the hydrophobic SAM [27]. The gold-coated slides were subsequently immersed in solutions containing poly(ethylene glycol) (PEG)-terminated alkanethiols to replace the etched regions with a hydrophilic PEG alkanethiolate SAM (Fig. 1a). Differential wettability of SAMs resulting from this removal and

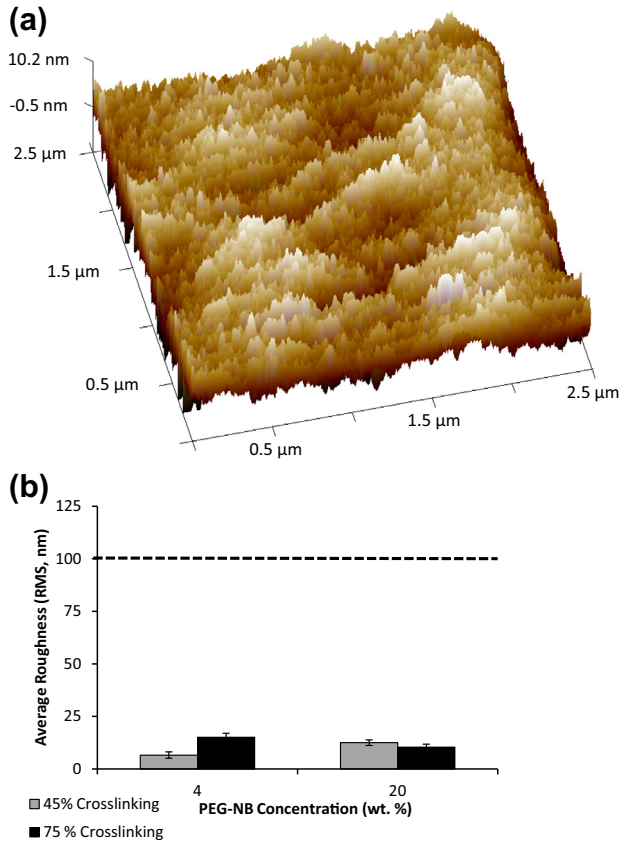

Fig. 2. Characterization of surface roughness of hydrogels formed using the array formation procedure. (a) Representative AFM height image of hydrogel (shown: 20 wt.%, 45% crosslinking) in liquid to determine the RMS roughness. (b) The calculated RMS roughness values (6.6–15.1 nm) for hydrogels with the lowest and highest stiffness values formed using this array formation procedure. Dotted line denotes minimum height used in previous studies investigating the influence of nanotopography of compliant surface on hMSC behavior. Sample size: $n = 3$ (b).

replacement method were confirmed using static contact angle measurements (Fig. 1b).

Hydrogel precursor solutions (0.75 μL per 2.4 mm diameter, 150 μm thick hydrogel spot) containing norbornene-functionalized PEG (PEG-NB) and PEG-dithiol (PEG-DT) were deposited onto the hydrophilic regions on the patterned gold-coated slide using either a single-channel micropipettor, multi-channel micropipettor, or a single-channel repeat pipettor. The wettability patterning was designed with dimensions compatible with an 8-channel micropipette, allowing for deposition of multiple solutions simultaneously. A 150 μm PDMS spacer was places on regions of the patterned gold slide and a silanized glass slide was placed atop the entire patterned gold slide to sandwich the precursor solution (Figs. 1c, d and A1a). UV-initiated crosslinking was used to form hydrogel spots via radically-mediated thiol-norbornene (term "thiolene") photopolymerization, a step-growth reaction mechanism that enabled rapid gelation time and resulted in homogeneous polymer network formation (Figs. 1e and 3a) [22,23]. The silanes on the silanized glass slide possessed terminal thiols that were capable of participating in thiolene reaction with the norbornene groups on PEG-NB, thereby enabling covalent immobilization of the hydrogels to the glass slide upon polymerization. The result was an array of hydrogel spots upon a glass slide (Fig. 1f). The dimensions of the hydrogel spots could be altered by changing the pattern on the elastomeric stencil used for SAM patterning (to define the *X* and *Y* dimensions) and by using a polydimethylsiloxane (PDMS) elastomeric spacer between the patterned SAM and the silanized glass slides (to define the *Z* dimension of the resulting hydrogel spot) (Fig. 1g and h). Note that the silanized glass slides promote non-specific cell adhesion which could contribute to the soluble factors presented in the microenvironment and influence cell behavior during

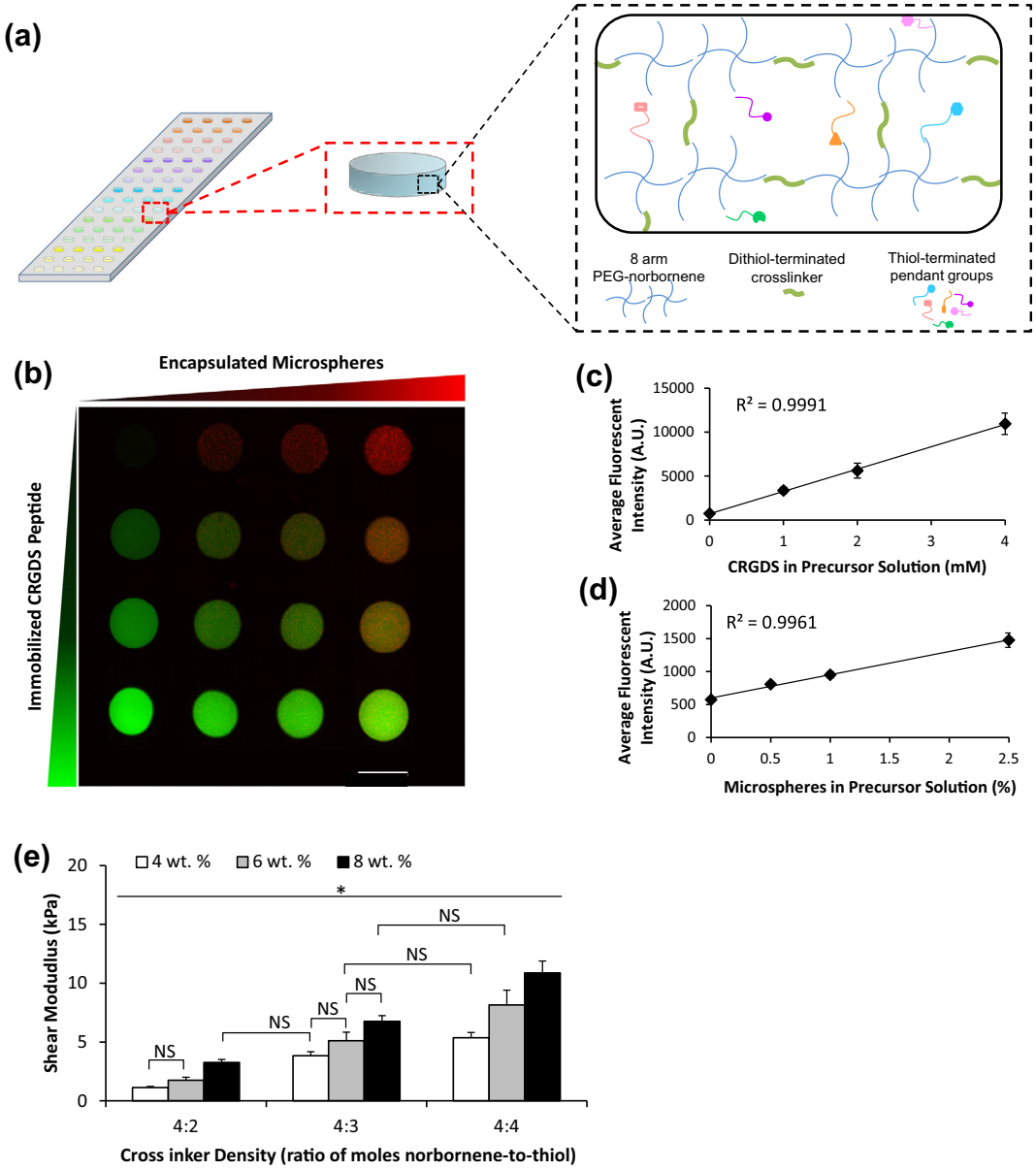

Fig. 3. Characterization of the chemical and mechanical properties of hydrogel spots in the array. (a) Schematic representation of array with hydrogel spots formed using thiolene chemistry. Array with hydrogel spots containing varying concentrations of immobilized CRGDS peptide (b and c) and encapsulated microspheres (b and d). Hydrogel spots with stiffness varied by changing concentration of PEG-NB or crosslinker density in the hydrogel precursor solution (e). Sample size: $n = 4$ (c and d) and $n = 3$ (e). Statistical significance was determined by two-factor ANOVA followed by Tukey HSD test, whereby * denotes statistical significant with $p < 0.05$ and "NS" denotes no statistical significance.

long-term cell culture. We are currently developing a passivation procedure to address this in our design process.

The lack of a liquid handling system does limit the throughput on this array formation method because of the time required for deposition of hydrogel precursor solution for each spot in the array. We use small volumes (0.75 μL) to generate each hydrogel spot to reduce the materials cost; however, due to the small volumes, evaporation concerns limited array sizes to what can be feasibly produced within a 5-min timeframe. Within a 5-min timeframe, we can feasibly generate an array for 2D culture comprised 80 spots formed using up to 16 different hydrogel precursor solutions. For 3D encapsulation studies, arrays sizes are limited by evaporation, cell viability in suspension, and cell settling once the hydrogel precursor solution has been deposited onto the patterned gold slide. Arrays formed for 3D encapsulation experiments in this manuscript were formed within 2 min and contained 20 spots formed using up to 5 different hydrogel precursor solutions.

Previous studies have indicated that natural and synthetic compliant surfaces with topographical features typically ⩾100 nm in height can be used to modulate integrin-mediated stem cell attachment, cytoskeletal structure, proliferation, migration, and differentiation [28–31]. As the hydrogel array formation procedure required glass-immobilized hydrogel detachment from the patterned gold-coated slide, it was plausible that this detachment could have contributed to the formation of nano- or micron-sized features on our hydrogel surface. Therefore, we used hydrated atomic force microscopy (AFM) to examine the resulting hydrogel surface roughness and root mean square (RMS) roughness of all hydrogels formed. Regardless of concentration of PEG-NB or PEG-DT crosslinker in the precursor solution, the surface roughnesses were similar in value and did not seem to correlate with changing PEG-NB or PEG-DT concentration (Fig. 2). This indicates that the detachment procedure and changes in hydrogel composition minimally influence surface nanotopography. Additionally, height of features found on our hydrogel surfaces (6.6–15.1 nm) are lower than the feature sizes commonly used in prior studies of surface topography effects, which suggests minimal contribution of surface topography to observed differences in hMSC behavior (Fig. 2b).

3.2. Changing composition of each hydrogel spot

The composition of each hydrogel spot in the arrays could be also systematically and independently altered (Fig. 3). Thiolene photopolymerization offered the advantage of facile ligand incorporation into the polymer network as long as the ligand contained a thiol capable of participating in thiolene reaction with PEG-NB (Fig. 3a). We utilized cysteine-terminated CRGDS peptide and, by changing the molar ratio of peptide to norbornene functional groups, we could systematically and independently change the concentration of the peptides immobilized in each hydrogel spot in the array (Fig. 3b and c). The resulting relative CRGDS concentrations in the hydrogel spots were directly correlated to the concentration of CRGDS in the hydrogel precursor solution ($R^2 = 0.9845$).

The array formation procedure also allowed for encapsulation of micron-sized materials and cells (Figs. 3b and 5). By adding the material or cells into the precursor solution, those components could be encapsulated within and uniformly distributed throughout the hydrogel spots upon photopolymerization (Fig. A2). As the mesh size of typical hydrogel networks generated were 6–12 nm (Fig. 4a), micron-sized components were not able to freely diffuse through and out of the network, thereby enabling their entrapment and encapsulation. We demonstrated the ability to change the density of encapsulated materials or cells by varying the concentration of fluorescently-tagged microspheres (from 0 to 2.5 w/v%) or cells (from 250,000 to 1 million cells/mL) in the hydrogel precursor solution (Figs. 3b, d and 5a–c). The resulting concentrations of encapsulated materials in the hydrogel spots were directly correlated to the concentrations of materials added to the hydrogel precursor solutions ($R^2 = 0.9855$ and 0.9655 for microspheres and cells, respectively). At the concentrations typically used for cell encapsulation studies (500,000 and 1 million cells/mL), the empirical cell number encapsulated in the hydrogels is 75% and 69% of the desired cell number. Note that, due to the small volumes of viscous fluids, low-resolution microscopy, and automated measurement techniques used to enable enhance throughput screening with the hydrogel arrays, minor technical errors could result in significant variability in the resulting encapsulated cell concentration. Consistent with other workflows utilizing screening techniques, results from enhanced throughput screens with our hydrogel arrays should be confirmed with follow-up experiments using large-scale culture.

We also demonstrated that the array formation procedure enabled hMSC encapsulation with cell viability consistent with those previous published for encapsulation in PEG hydrogels (70–90% viable cells at 24 h after encapsulation, Fig. 5d–e) [8,32,33]. Additionally, increasing concentration of CRGDS (which has been used to promote hMSC adhesion to hydrogel surfaces through interactions with $\alpha_v\beta_3$ and $\alpha_5\beta_1$ integrins on the cell surface) did not significantly affect hMSC viability (Fig. 5e) [33–35].

The hydrogel spot stiffness (as measured by shear storage modulus) was controllably altered by varying either the concentration of PEG-NB or PEG-DT crosslinker in the precursor solution. These results were consistent with those previously reported [36]. Hydrogel shear modulus was directly correlated to both PEG-NB monomer concentration and PEG-DT crosslinker density (with

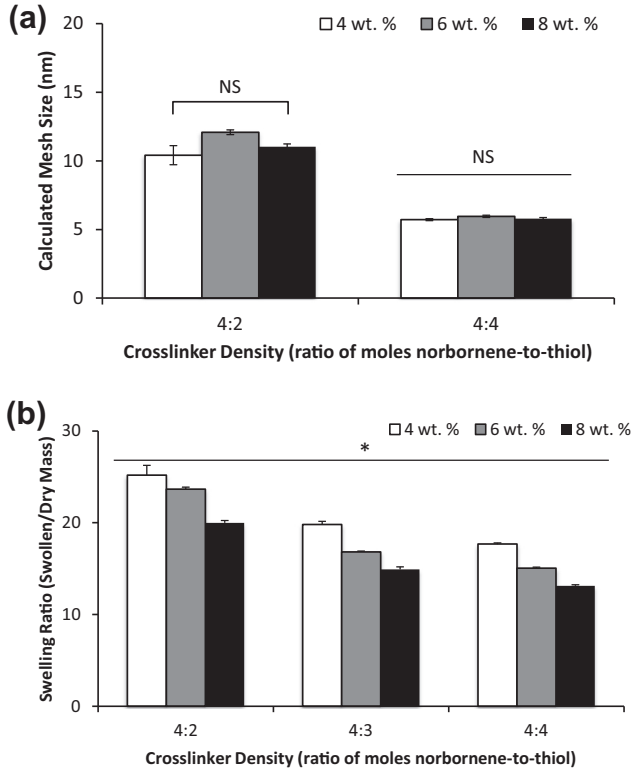

Fig. 4. Characterization of hydrogel physical properties and network structure. (a) Hydrogel network mesh size predicted using calculations based on Flory–Rehner theory. (b) Mass equilibrium swelling ratio of bulk hydrogels formed with varying PEG-NB (wt.%) and crosslinker density. Sample size: $n = 3$ (a and b). Statistical significance was determined by two-factor ANOVA followed by Tukey HSD test, whereby * denotes statistical significant with $p < 0.05$ and "NS" denotes no statistical significance.

50–100% density corresponding to 0.5–1 mol ratio of thiol-to-norbornene) in the precursor solution, and these results were confirmed by determining equilibrium mass swelling ratio (Figs. 3e and 4b).

3.3. hMSC adhesion and proliferation on hydrogel array

For hMSC adhesion studies, we generated arrays containing hydrogel spots with stiffness values ranging from 1.8 to 10.9 kPa and varying immobilized CRGDS peptide concentrations from 0 to 4 mM. The arrays generated comprised several isolated hydrogel spots where each hydrogel spot possessed a unique CRGDS concentration and stiffness value. As the PEG hydrogel is bio-inert and does not permit cell adhesion, the inclusion of RGD-containing peptides was designed to promote hMSC integrin-mediated cell adhesion and enable integrin-mediated mechanosensing [14,21,22,37,38]. Note that total peptide concentration was maintained at 4 mM by supplementing the hydrogel precursor solution with a "scrambled", non-bioactive CRDGS peptide (whereby "0 mM CRGDS" hydrogels contain 4 mM CRDGS scrambled peptide). The stiffness range was chosen to reflect the reported stiffness values of various soft tissues, including fat and muscle tissue [39,40]. Following hydrogel array formation, hMSCs were seeded onto the hydrogel spots and cultured for up to 8 days (Fig. 6a). hMSC initial cell attachment, spreading, and proliferation were linearly correlated with immobilized CRGDS concentration (Figs. 6b–d and A3a–d) regardless of the hydrogel spot stiffness. After 1 day of culture, minimal hMSCs were attached to hydrogel spots that did not contain CRGDS (4 mM "scrambled" CRDGS), indicating that initial cell adhesion was mediated by the bioactivity of the immobilized peptide. Increased CRGDS concentration resulted in increased hMSC attachment, spreading, and proliferation with

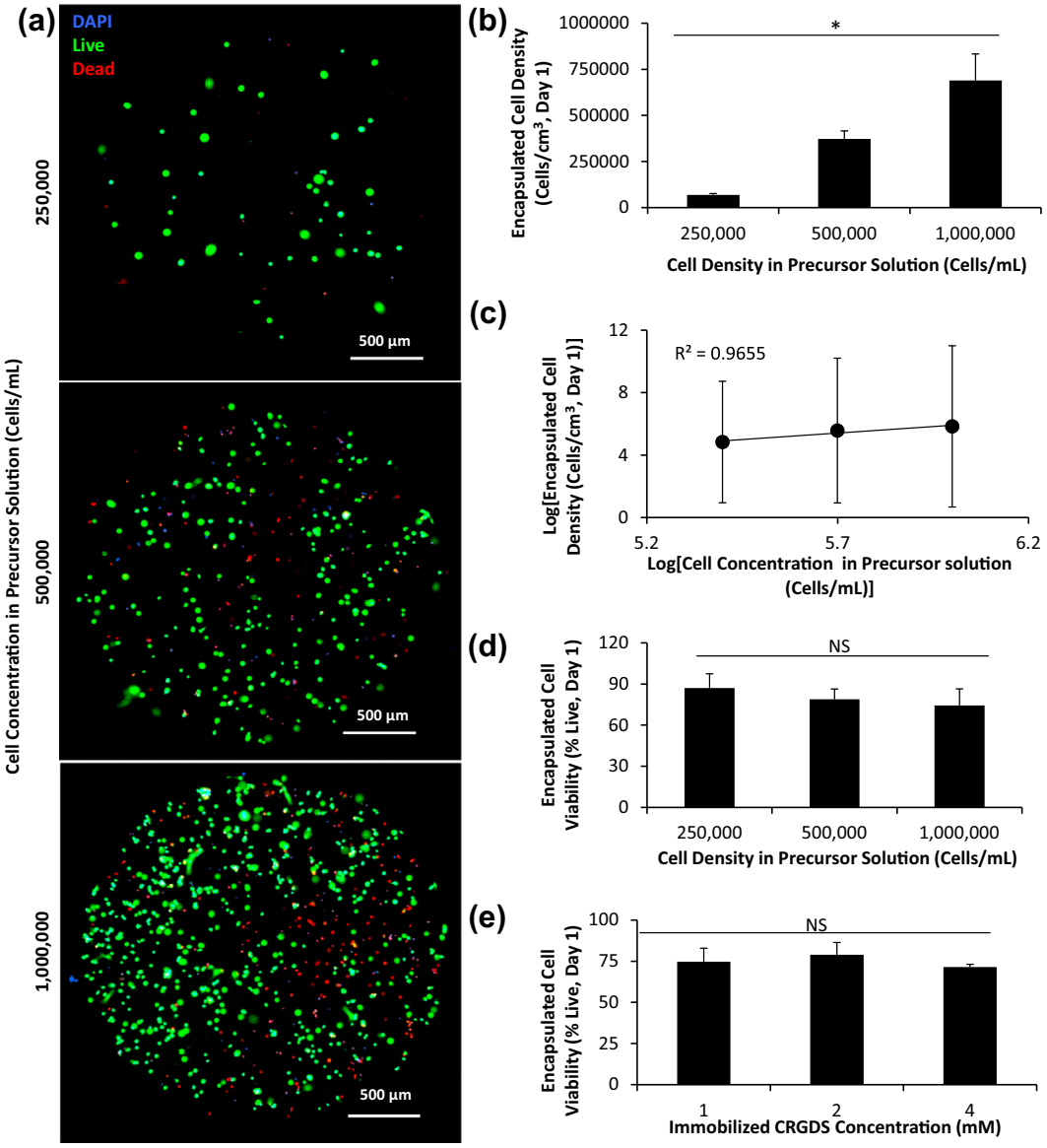

Fig. 5. Demonstration of hMSC encapsulation in hydrogels formed using differential wettability patterning. All hydrogels presented CRGDS and were crosslinked with a MMP-degradable peptide. (a–d) Viability and density of hMSCs encapsulated in hydrogel spots presenting 2 mM CRGDS and formed using precursor solutions with varying concentrations of hMSC. (a) Maximum intensity projection created by stacking images of the hydrogel acquired at 3 different focal planes in the hydrogel. (c) Correlation of encapsulated hMSC density with hMSC concentration in precursor solution. (e) Viability of ~500,000 hMSCs encapsulated in hydrogels spots containing varying concentrations of immobilized CRGDS peptide. Sample size: $n \geqslant 5$ (b, d, e), $n = 3$ (c). Statistical significance was determined by ANOVA followed by Tukey–Kramer test, whereby * denotes $p < 0.05$ and "NS" denotes no statistical significance.

maximal values on hydrogel spots presenting 4 mM CRGDS. These results are consistent with previously reported relationships [12,13,18,24,41], and confirmed that hydrogel arrays can be used to screen for the effects of peptide density and identity on hMSC behavior.

Increasing hydrogel spot stiffness (from 1.8 to 10.9 kPa) also resulted in increased hMSC initial cell attachment, spreading, and proliferation; however, maximal values for these cell behaviors were achieved on hydrogel spots with the highest CRGDS concentration and intermediate stiffness values Fig. 6b–d). In particular, maximal hMSC initial cell attachment was seen on hydrogel spots of 8.2 kPa stiffness while maximal cell spreading and proliferation were both seen on hydrogel spots of 5.4 kPa stiffness. As previous studies have reported that hMSC integrin-mediated mechanosensing is directly correlated to cytoskeletal tension, we examined focal adhesion formation and cytoskeletal structure to assess the influence of hydrogel spot stiffness on cytoskeletal tension [10,12,13,15,16,18,38]. Immunofluorescence staining for vinculin (a component of focal adhesions) and F-actin (an important component of stress fibers in adherent cultured cells) qualitatively revealed diffuse F-actin and focal adhesion in hMSCs seeded on softer hydrogels spots (3.3 kPa or less), while those seeded on stiffer hydrogels spots (5.4 kPa or greater) expressed well-defined stress fibers terminated by prominent focal adhesions (Fig. 7a). hMSCs expression of F-actin stress fibers terminated by prominent focal adhesions has been previously directly correlated to both substrate stiffness and cytoskeletal tension [10,15,16,18]. Independent of CRGDS concentration and substrate stiffness, hMSCs cultured on all substrates used in this study present mature focal adhesions ($\geqslant$5 μm in length, Fig. 7) [31]. Independent of substrate stiffness, hMSC focal adhesion density appeared to be linearly correlated to CRGDS concentration (R^2 = 0.8852, Fig. 7b). Additionally, independent of CRGDS concentration, focal adhesion length appeared to be correlated with substrate stiffness (Fig. 7c). These trends are consistent with those previously reported and further support that hydrogel spot stiffness can be used to modulate hMSC cytoskeletal tension [42,43]. Combined, these results suggested that hydrogel arrays produced here may be used to screen for the effects of substrate stiffness on hMSC mechanosensing.

Interestingly, examination of the combinatorial effects of CRGDS concentration and hydrogel spot stiffness revealed potential interplay between these distinct substrate signals. The synergy between adhesion and stiffness is most clearly demonstrated with hMSC proliferation (Fig. 6d). At 4 mM CRGDS, hMSCs proliferate regardless of hydrogel spot stiffness; however, hydrogel spots presenting 1 and 2 mM CRGDS required stiffness values greater than 1.8 and 3.3 kPa, respectively. These results are consistent with previously reported trends suggesting that low cytoskeletal tension in response to low cell adhesion ligand density could be compensated by high cytoskeletal tension produced from high substrate stiffness [12,13]. Additionally, these trends suggest some baseline level of cytoskeletal tension was required for hMSC proliferation on hydrogel substrates and that multiple substrate signals could be engineered to work in synergy to promote mechanosensing and regulate cell behavior [5,13]. It is worthwhile to note that, as we modified both PEG-NB concentration and crosslinking density to control stiffness, it is unclear the extent to which stiffness influences surface polymer chain mobility and subsequently the ability for the cells to access the cell adhesive ligands. Increasing stiffness could potentially decrease polymer chain mobility, reduce the effective CRGDS density accessible to the cells, and actively limit integrin clustering which subsequently impacts hMSC cytoskeletal reorganization and mechanosensing. Previous studies indicated that integrin clustering regulates cell adhesion, spreading, and proliferation and are dependent on both concentration and spatial distribution of cell adhesive ligands [31,44]. Increasing PEG-NB concentration and crosslinking density could reduce polymer chain mobility to decrease the number of favorable conformations of the CRGDS ligand during integrin clustering, thereby limiting the cluster size and distribution on the cell surface. Additionally,

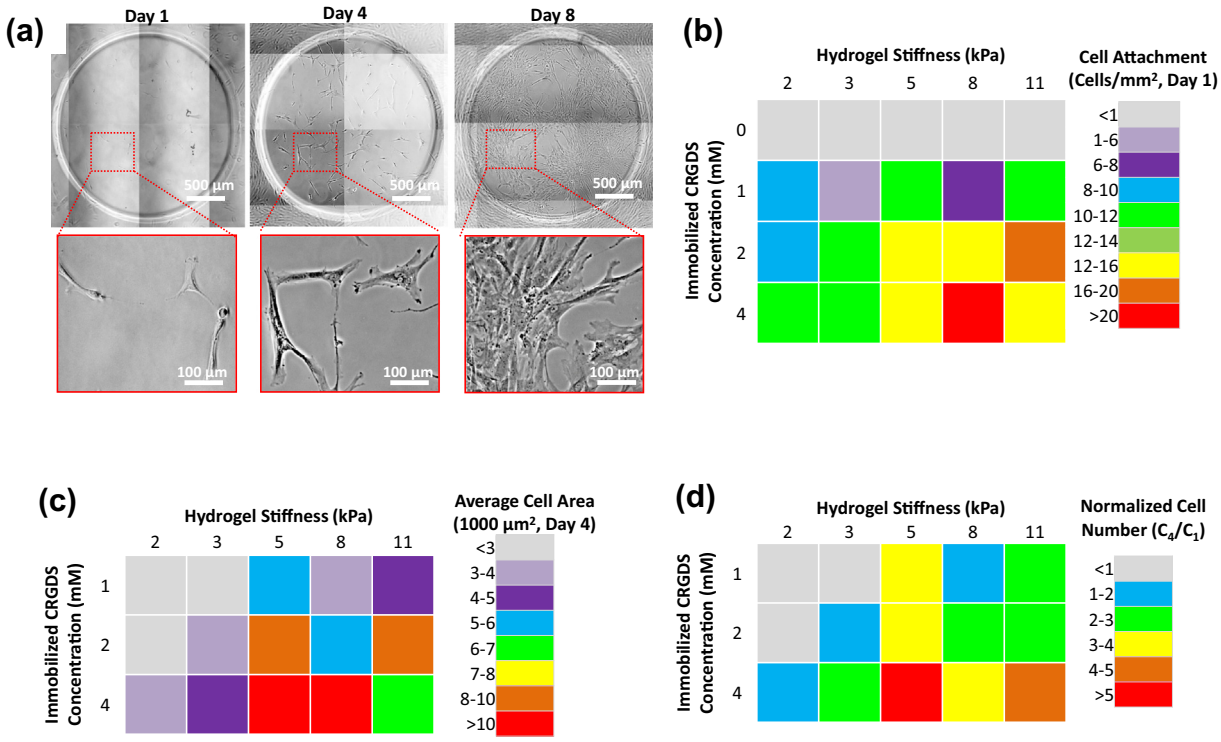

Fig. 6. Effects of hydrogel spot stiffness and immobilized CRGDS concentration on hMSC behavior. (a) hMSC culture on hydrogel spots presenting 4 mM CRGDS over the course of 8 days. hMSC (b) cell attachment one day after cell seeding, (c) cell spreading four days after cell seeding, and (d) cell proliferation (indicated by normalized cell number from day 4 compared to day 1, $C_4/C_1 > 1$) after four days of culture sample size: $n = 4$ (b–d).

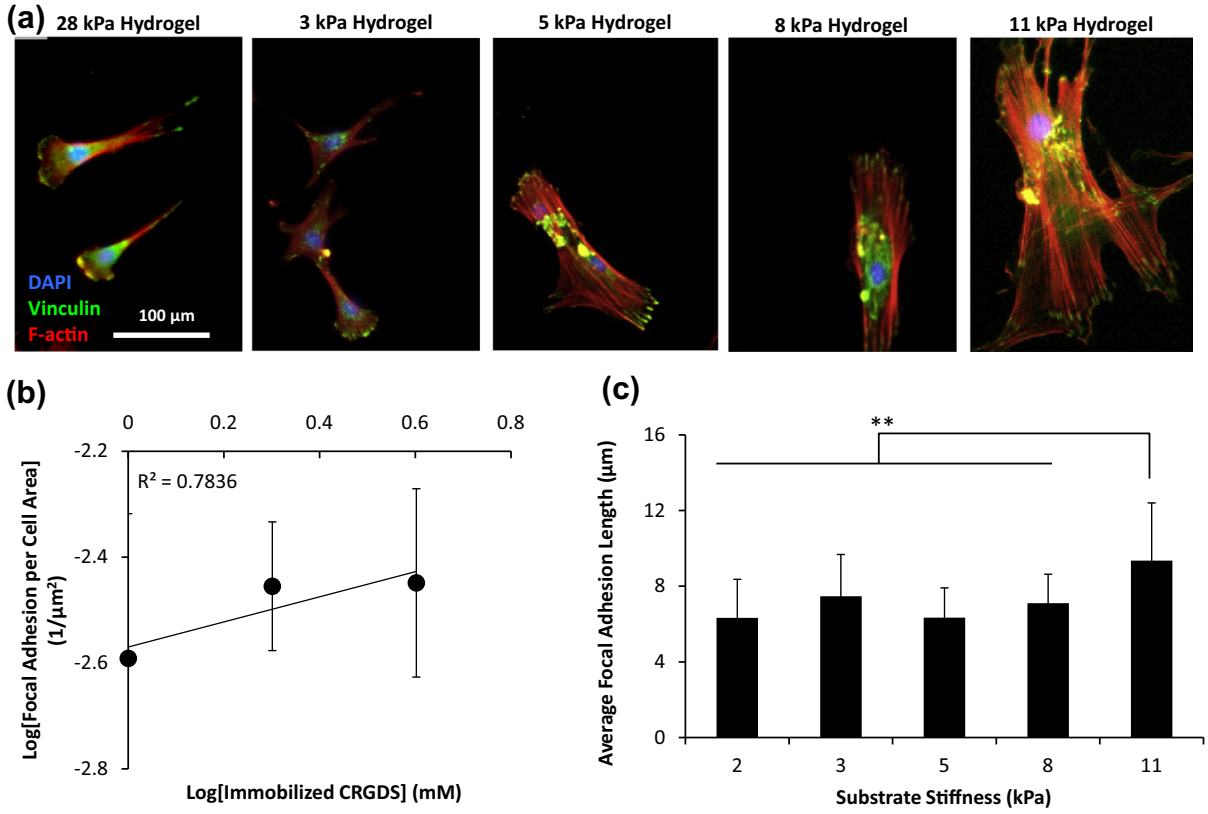

Fig. 7. Effects of hydrogel spot stiffness and immobilized CRGDS concentration on hMSC cytoskeletal structure. (a) Focal adhesion (vinculin, green), stress fiber (F-actin, red), and nuclear (DAPI, blue) stain of hMSCs after 8 days of culture on hydrogel spots with varying stiffness and presenting 4 mM CRGDS. (b) Correlation of hMSC focal adhesion density with immobilized CRGDS concentration (calculated by averaging all hydrogel spots with the same CRGDS concentration, regardless of stiffness). (c) Average hMSC focal adhesion length on hydrogels of different stiffness values (calculated by averaging all hydrogel spots with the same stiffness values, regardless of CRGDS concentration). Sample size: $n \geqslant 25$ (b and c). Asterisks denote statistical significance as determined by single factor ANOVA followed by Tukey–Kramer test, whereby $^{**}p < 0.01$. (For interpretation of the references to color in this figure legend, the reader is referred to the web version of this article.)

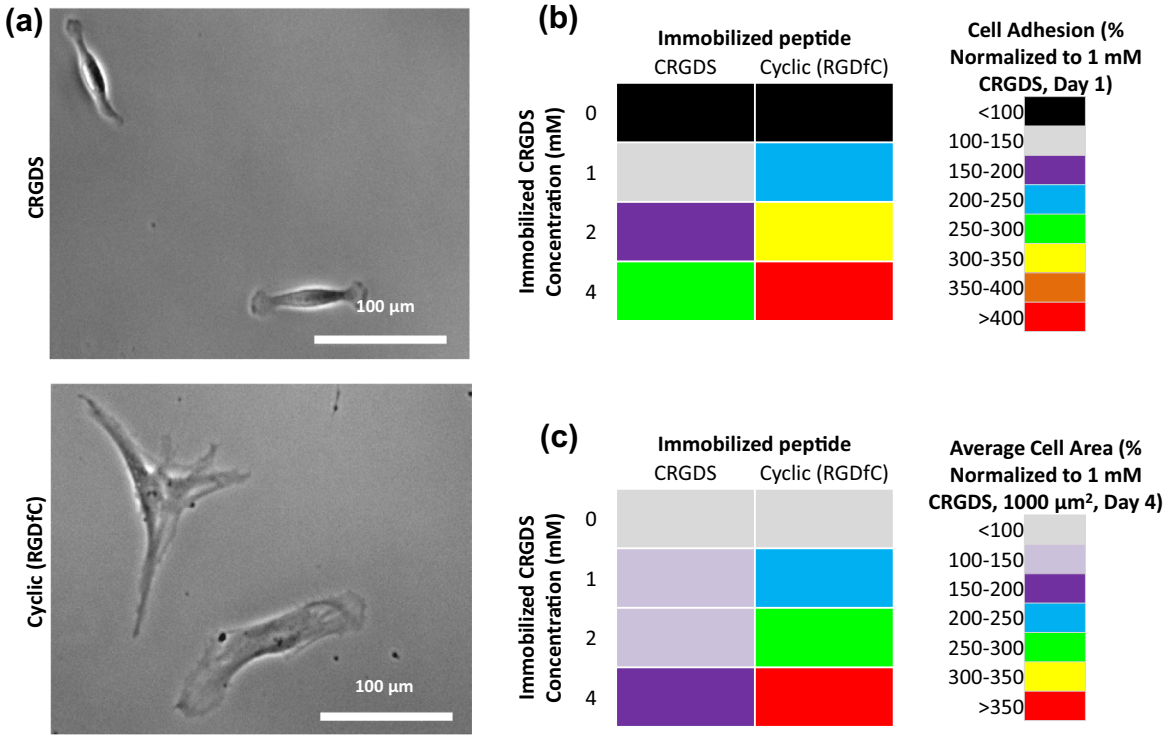

Fig. 8. Effects of immobilized peptide identity on hMSC behavior. (a) hMSC attachment on hydrogels presenting linear CRGDS or cyclic (RGDfC) after 3 days of culture. (b) hMSC cell attachment one day after seeding and (c) cell spreading after 3 days culture on hydrogel spots presenting 4 mM CRGDS or cyclic (RGDfC). Sample size: $n \geqslant 6$ (b and c).

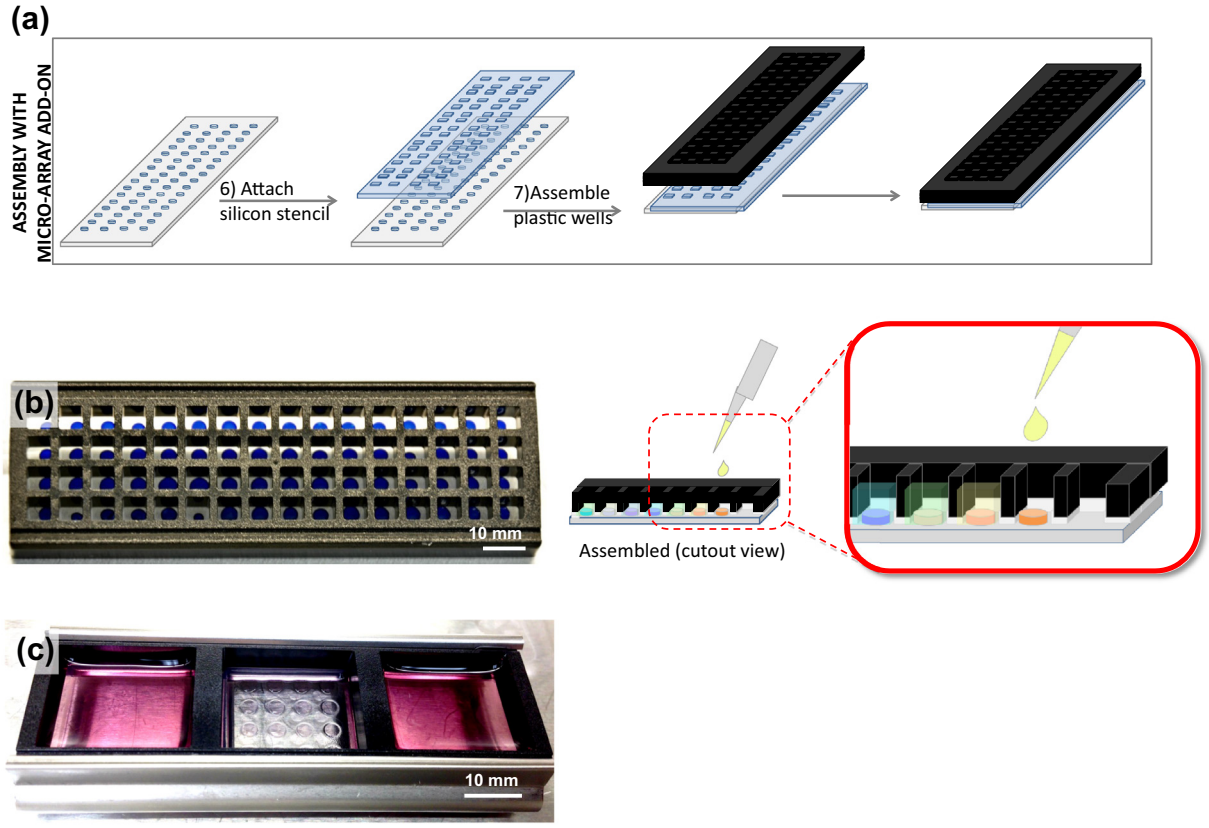

Fig. 9. Demonstration of hydrogel array setup for soluble media screening. (a) Hydrogel array assembly with commercially-available micro-array add-on for ability to introduce different soluble factors to (b) each individual spot or (c) group of spots in the array. (b and c) Hydrogels stained with Trypan blue and media contains phenol red for enhanced contrast and visibility. (For interpretation of the references to color in this figure legend, the reader is referred to the web version of this article.)

increasing crosslinking density could decrease potential sites for CRGDS covalently attachment and subsequently reduce effective CRGDS density [31]. Previous studies have also suggested that integrin clustering and mechanosensing is dependent on the flexibility of the anchor points to which cells adhere to the surface [31,38,44]. By increasing crosslinking density to increase substrate stiffness, we could have potentially decreased anchor point flexibility and limited hMSC integrin clustering, leading to increase hMSC spreading on stiffer substrates.

3.4. hMSC adhesion on hydrogels presenting peptides with varying ligand–receptor affinity

We cultured hMSCs on hydrogels spots presenting 0–4 mM of the linear CRGDS or the cyclic (RGDfC) peptide to determine the influence of ligand–receptor affinity on cell behavior (Fig. 8). Previous studies have indicated that the cyclic peptide possesses higher affinity for $\alpha_v\beta_3$ integrins than the linear peptide [34,35]. Note that total peptide concentration was maintained at 4 mM by supplementing the hydrogel precursor solutions with the non-bioactive CRDGS peptide. Following hydrogel array formation, hMSCs were seeded onto the hydrogel spots and cultured for up to 3 days (Fig. 8a). While changing the immobilize peptide identity did not significantly change the hydrogel spot stiffness or the linear correlation between both initial hMSC attachment or spreading and immobilized RGD-containing peptide concentration (Fig. A4), hMSCs initial attachment and spreading on hydrogels presenting cyclic (RGDfC) was higher than on hydrogels presenting equivalent concentrations of CRGDS (Fig. 8b). These results are consistent with those previously reported for comparison of hMSC attachment and spreading on SAMs presenting linear vs. cyclic RGD-containing peptides [13] and suggest that hydrogels with varying immobilized peptides identity could be used to screen for the effects of changing ligand–receptor affinity on hMSC mechanosensing.

It is worthwhile to note that previous studies have suggested that more low-affinity ligands must be presented to the cells in order to achieve the same integrin clustering, stable attachments, and cell spreading when compared to higher affinity ligands [31]. Consistent with these suggestions, low concentrations of cyclic (RGDfC) promoted similar or higher levels of hMSC initial attachment and spreading than high concentrations of CRGDS (Fig. 8b and c).

4. Conclusion

In conclusion, we have developed a method for forming hydrogel arrays using surfaces patterned with differential wettability. The proof-of-concept study presented here confirmed that our hydrogel array formation procedure is capable of producing hydrogel spots with properties that can be systematically and independently varied and that these arrays can be used for stem cell culture and screening for the effects of various chemical and mechanical substrate properties on stem cell behavior. While we and others have previously developed other hydrogel array systems for stem cell culture and screening [2,6,7,21,37,45], our current array system offers the unique advantage of benchtop array formation for both 2- and 3-dimensional cell cultures and enhanced-throughput screening without the need for liquid handling systems [7]. Our method is also suitable for screening the

influence of substrate size, shape, and thickness on stem cell behavior via our ability to control the *XYZ* dimensions. Additionally, hydrogel arrays formed using our method are compatible with commercially-available micro-array add-on systems, thereby enabling attachment of wells for each individual spots to offer control over the soluble medium presented to each spot in the array (Fig. 9). Our hydrogel array system therefore can be used to identify and optimize substrate properties and culture conditions for stem cell culture. This capability is particularly important in stem cell engineering, as there is a need for optimization of chemically well-defined cell culture substrates for stem cell expansion, differentiation, and tissue assembly.

Acknowledgments

The authors acknowledge the following funding sources: the National Institutes of Health (Grant No. R01HL093282), the National Science Foundation (Grant No. 1306482), the National Science Foundation Graduate Research Fellowships Program (Grant No. DGE-0718123), the University of Wisconsin-Madison Graduate Engineering Research Scholars, and the Gates Millennium Scholars Program. The authors also acknowledge support from staff and the use of equipment at the Materials Science Center (National Science Foundation Grant No. 1121288) and services from the National Magnetic Resonance Facility at the University of Wisconsin-Madison.

Appendix A. Supplementary data

Supplementary data associated with this article can be found, in the online version, at http://dx.doi.org/10.1016/j.actbio.2015.09.019.

References

[1] Y. Sun, C.S. Chen, J. Fu, Forcing stem cells to behave: a biophysical perspective of the cellular microenvironment, Ann. Rev. Biophys. 41 (2012) 519–542.
[2] S. Gobaa, S. Hoehnel, M. Roccio, A. Negro, S. Kobel, M.P. Lutolf, Artificial niche microarrays for probing single stem cell fate in high throughput, Nat. Methods 8 (2011) 949–955.
[3] D.E. Discher, D.J. Mooney, P.W. Zandstra, Growth factors, matrices, and forces combine and control stem cells, Science 324 (2009) 1673–1677.
[4] O.Z. Fisher, A. Khademhosseini, R. Langer, N.A. Peppas, Bioinspired materials for controlling stem cell fate, Acc. Chem. Res. 43 (2010) 419–428.
[5] J. Lee, A.A. Abdeen, D. Zhang, K.A. Kilian, Directing stem cell fate on hydrogel substrates by controlling cell geometry, matrix mechanics and adhesion ligand composition, Biomaterials 34 (2013) 8140–8148.
[6] L. Jongpaiboonkit, W.J. King, W.L. Murphy, Screening for 3D environments that support human mesenchymal stem cell viability using hydrogel arrays, Tissue Eng. Part A 15 (2009) 11.
[7] A. Ranga, M.P. Lutolf, High-throughput approaches for the analysis of extrinsic regulators of stem cell fate, Curr. Opin. Cell Biol. 24 (2012) 236–244.
[8] W.J. King, L. Jongpaiboonkit, W.L. Murphy, Influence of FGF2 and PEG hydrogel matrix properties on hMSC viability and spreading, J. Biomed. Mater. Res. Part A 93A (2010) 1110–1123.
[9] L. Jongpaiboonkit, W.J. King, G.E. Lyons, A.L. Paguirigan, J.W. Warrick, D.J. Beebe, et al., An adaptable hydrogel array format for 3-dimensional cell culture and analysis, Biomaterials 29 (2008) 3346–3356.
[10] A.J. Engler, S. Sen, H.L. Sweeney, D.E. Discher, Matrix elasticity directs stem cell lineage specification, Cell 126 (2006) 677–689.
[11] A.J. Engler, L. Bacakova, C. Newman, A. Hategan, M. Griffin, D.E. Discher, Substrate compliance versus ligand density in cell on gel responses, Biophys. J. 86 (2004) 617–628.
[12] A.K. Jha, K.E. Healy, Controlling osteogenic stem cell differentiation via soft, PLoS ONE 9 (2014) 1–11.
[13] K.A. Kilian, M. Mrksich, Directing stem cell fate by controlling the affinity and density of ligand-receptor interactions at the biomaterials interface, Angew. Chem. 51 (2012) 4891–4895.
[14] J.H. Wen, L.G. Vincent, A. Fuhrmann, Y.S. Choi, K.C. Hribar, H. Taylor-Weiner, et al., Interplay of matrix stiffness and protein tethering in stem cell differentiation, Nat. Mater. 13 (2014) 979–987.
[15] N.R. Gandavarapu, D.L. Alge, K.S. Anseth, Osteogenic differentiation of human mesenchymal stem cells on alpha5 integrin binding peptide hydrogels is dependent on substrate elasticity, Biomater. Sci. 2 (2014) 352–361.
[16] M. Guvendiren, J.A. Burdick, Stiffening hydrogels to probe short- and long-term cellular responses to dynamic mechanics, Nat. Commun. 3 (2012) 792.
[17] S.Y. Tee, J. Fu, C.S. Chen, P.A. Janmey, Cell shape and substrate rigidity both regulate cell stiffness, Biophys. J. 100 (2011). L25-7.
[18] J.T. Koepsel, S.G. Loveland, M.P. Schwartz, S. Zorn, D.G. Belair, N.N. Le, et al., A chemically-defined screening platform reveals behavioral similarities between primary human mesenchymal stem cells and endothelial cells, Integr. Biol.: Quant. Biosci. Nano Macro 4 (2012) 1508–1521.
[19] C.R. Vistas, A.C.P. Águas, G.N.M. Ferreira, Silanization of glass chips—a factorial approach for optimization, Appl. Surf. Sci. 286 (2013) 314–318.
[20] I.E. Dunlop, S. Zorn, G. Richter, V. Srot, M. Kelsch, P.A. van Aken, et al., Titanium–silicon oxide film structures for polarization-modulated infrared reflection absorption spectroscopy, Thin Solid Films 517 (2009) 2048–2054.
[21] E.H. Nguyen, M.R. Zanotelli, M.P. Schwartz, W.L. Murphy, Differential effects of cell adhesion, modulus and VEGFR-2 inhibition on capillary network formation in synthetic hydrogel arrays, Biomaterials 35 (2014) 2149–2161.
[22] B.D. Fairbanks, M.P. Schwartz, A.E. Halevi, C.R. Nuttelman, C.N. Bowman, K.S. Anseth, A versatile synthetic extracellular matrix mimic via thiol-norbornene photopolymerization, Adv. Mater. 21 (2009) 5005–5010.
[23] M.W. Toepke, N.A. Impellitteri, J.M. Theisen, W.L. Murphy, Characterization of thiol-ene crosslinked PEG hydrogels, Macromol. Mater. Eng. 298 (2013) 699–703.
[24] S. Lin, N. Sangaj, T. Razafiarison, C. Zhang, S. Varghese, Influence of physical properties of biomaterials on cellular behavior, Pharm. Res. 28 (2011) 1422–1430.
[25] N.A. Peppas, E.W. Merrill, Poly(vinyl Alcohol) hydrogels: reinforcement of radiation-crosslinked networks by crystallization, J. Polym. Sci. 14 (1976) 441–457.
[26] T. Canal, N.A. Peppas, Correlation between mesh size and equilibrium degree of swelling of polymeric networks, J. Biomed. Mater. Res. 23 (1989) 1183–1193.
[27] J.T. Koepsel, W.L. Murphy, Patterned self-assembled monolayers: efficient, chemically defined tools for cell biology., Chembiochem: Eur. J. Chem. Biol. 13 (2012) 1717–1724.
[28] L.E. McNamara, R.J. McMurray, M.J.P. Biggs, F. Kantawong, R.O.C. Oreffo, M.J. Dalby, Nanotopographical control of stem cell differentiation, J. Tissue Eng. 1 (2010) 120623.
[29] F. Guilak, D.M. Cohen, B.T. Estes, J.M. Gimble, W. Liedtke, C.S. Chen, Control of stem cell fate by physical interactions with the extracellular matrix, Cell Stem Cell 5 (2009) 17–26.
[30] L.-A. Turner, M.J. Dalby, Nanotopography – potential relevance in the stem cell niche, Biomater. Sci. 2 (2014) 1574–1594.
[31] M.J. Dalby, N. Gadegaard, R.O.C. Oreffo, Harnessing nanotopography and integrin-matrix interactions to influence stem cell fate, Nat. Mater. 13 (2014) 558–569.
[32] A. Raza, C.-C. Lin, The influence of matrix degradation and functionality on cell survival and morphogenesis in PEG-based hydrogels, Macromol. Biosci. 13 (2013) 1048–1058.
[33] C.R. Nuttelman, M.C. Tripodi, K.S. Anseth, Synthetic hydrogel niches that promote hMSC viability, Matrix Biol. 24 (2005) 208–218.
[34] E. Ruoslahti, RGD and other recognition sequences for integrins, Annu. Rev. Cell Dev. Biol. 12 (1996) 697–715.
[35] R. Haubner, D. Finsinger, H. Kessler, Stereoisomeric peptide libraries and peptidomimetics for designing selective inhibitors of the αvβ3 integrin for a new cancer therapy, Angew. Chem. Int. Ed. Engl. 36 (1997) 1374–1389.
[36] A.K. Jha, W.M. Jackson, K.E. Healy, Controlling osteogenic stem cell differentiation via soft bioinspired hydrogels, PLoS ONE 9 (2014) 1–11.
[37] M.J. Wilson, Y. Jiang, B. Yañez-Soto, S. Liliensiek, W.L. Murphy, P.F. Nealey, Arrays of topographically and peptide-functionalized hydrogels for analysis of biomimetic extracellular matrix properties, J. Vac. Sci. Technol. B Nanotechnol. Microelectron.: Mater. Process. Meas. Phenom.: JVST B 30 (2012) 06F903.
[38] B. Trappmann, J.E. Gautrot, J.T. Connelly, D.G. Strange, Y. Li, M.L. Oyen, et al., Extracellular-matrix tethering regulates stem-cell fate, Nat. Mater. 11 (2012) 642–649.
[39] A. Geerligs, G.W. Peters, P.A. Ackermans, C.W. Oomens, Linear viscoelastic behavior of subcutaneous adipose tissue, Biorheology 45 (2008) 677–688.
[40] A. Nordez, F. Hug, Muscle shear elastic modulus measured using supersonic shear imaging is highly related to muscle activity level, J. Appl. Physiol. 108 (2010) 1389–1394.
[41] S.K. Schmitt, W.L. Murphy, P. Gopalan, Crosslinked PEG mats for peptide immobilization and stem cell adhesion, J. Mater. Chem. B 1 (2013) 1349.
[42] G. Geiger, A. Bershadsky, R. Pankov, K.M. Yamada, Transmembrane extracellular matrix-cytoskeleton crosstalk, Nat. Rev. Mol. Cell Biol. 2 (2001) 793–805.
[43] J.M. Goffin, P. Pittet, G. Csucs, J.W. Lussi, J.J. Meister, B. Hinz, Focal adhesion size controls tension-dependent recruitment of alpha-smooth muscle actin to stress fibers, J. Cell Biol. 172 (2006) 259–268.
[44] H.J. Kong, T. Boontheekul, D.J. Mooney, Quantifying the relation between adhesion ligand–receptor bond formation and cell phenotype, Proc. Natl. Acad. Sci. USA 103 (2006) 18534–18539.
[45] A. Khademhosseini, R. Langer, J. Borenstein, J.P. Vacanti, Microscale technologies for tissue engineering and biology, Proc. Natl. Acad. Sci. USA 103 (2006) 2480–2487.